

1 **Elucidating the acid-base mechanisms underlying otolith overgrowth in fish**
2 **exposed to ocean acidification**

3

4 Garfield T. Kwan^{1,2*}, Martin Tresguerres^{1*}

5 ¹Marine Biology Research Division, Scripps Institution of Oceanography, University of
6 California San Diego, USA

7 ²NOAA Fisheries Service, Southwest Fisheries Science Center, USA

8 *Corresponding authors: gkwan@ucsd.edu; mtresguerres@ucsd.edu

9

10 **Abstract**

11 Over a decade ago, ocean acidification (OA) exposure was reported to induce
12 otolith overgrowth in teleost fish. This phenomenon was subsequently confirmed in
13 multiple species; however, the underlying physiological causes remain unknown. Here,
14 we report that splitnose rockfish (*Sebastodes diploproa*) exposed to ~1,600 μatm $p\text{CO}_2$
15 (pH ~7.5) were able to fully regulate the pH of both blood and endolymph (the fluid that
16 surrounds the otolith within the inner ear). However, while blood was regulated around
17 pH 7.80, the endolymph was regulated around pH ~8.30. These different pH setpoints
18 result in increased $p\text{CO}_2$ diffusion into the endolymph, which in turn leads to
19 proportional increases in endolymph $[\text{HCO}_3^-]$ and $[\text{CO}_3^{2-}]$. Endolymph pH regulation
20 despite the increased $p\text{CO}_2$ suggests enhanced H^+ removal. However, a lack of
21 differences in inner ear bulk and cell-specific Na^+/K^+ -ATPase and vacuolar type H^+ -
22 ATPase protein abundance localization pointed out to activation of preexisting
23 ATPases, non-bicarbonate pH buffering, or both, as the mechanism for endolymph pH-

24 regulation. These results provide the first direct evidence showcasing the acid-base
25 chemistry of the endolymph of OA-exposed fish favors otolith overgrowth, and suggests
26 that this phenomenon will be more pronounced in species that count with more robust
27 blood and endolymph pH regulatory mechanisms.

28

29 **Keywords**

30 Endolymph, climate change, calcification, biomineralization, rockfish, carbon dioxide

31

32 **Introduction**

33 The inner ear of teleost fishes contains three pairs of otoliths that contribute to
34 hearing and maintaining balance. Otoliths are comprised of calcium carbonate (CaCO_3)
35 embedded within a protein matrix, and are biomineralized within an acellular fluid called
36 the endolymph (Payan et al., 2004a). Otoliths are biomineralized in a successive ring
37 pattern correlated with the fish growth rate (Campana and Neilson, 1985; Kalish, 1989;
38 Pannella, 1971), which are used by scientists and fishery managers to estimate fish age
39 and length (Campana, 2001; Campana and Thorrold, 2001), estimate recruitment, and
40 set fishery-specific catch limits (Methot, 2015; Vitale et al., 2019).

41 Originally, it was predicted that CO_2 -induced ocean acidification (OA) would
42 impair otolith biomineralization because the associated decreases in seawater pH and
43 $[\text{CO}_3^{2-}]$ hamper CaCO_3 precipitation (Ishimatsu et al., 2008). However, subsequent
44 studies reported that fish exposed to OA developed enlarged otoliths (S. Bignami et al.,
45 2013; Sean Bignami et al., 2013; Checkley et al., 2009; Faria et al., 2017; Hurst et al.,
46 2012; Réveillac et al., 2015; Shen et al., 2016). These findings led to a broader

47 awareness that otolith biomineralization is strongly linked to endolymph and blood
48 chemistries, and to the hypothesis that biological regulation of endolymph pH could lead
49 to increased $[CO_3^{2-}]$ resulting in otolith overgrowth (Checkley et al., 2009). In addition,
50 fish exposed to hypercapnia typically accumulate $[HCO_3^-]$ in their plasma to compensate
51 the respiratory acidosis; this could result in enhanced HCO_3^- flux into the endolymph
52 and further contribute to otolith overgrowth (Heuer and Grosell, 2014). However,
53 experimental support for these hypotheses is lacking, as there are no reports of
54 endolymph acid-base parameters under OA-relevant conditions, and only a few studies
55 have measured blood acid-base parameters in fish exposed to OA-relevant CO_2 levels
56 (Esbaugh et al., 2016, 2012; Montgomery et al., 2019). This knowledge gap is in large
57 part due to the disrupting effects of blood sampling by caudal puncture on the acid-base
58 status of fish internal fluids and the challenge of blood vessel cannulation in small fish
59 and species with convoluted dorsal aorta anatomy, coupled with the difficulty of
60 collecting sufficient endolymph for analyses. Moreover, the cellular heterogeneity of the
61 inner ear complicates the quantification of ionocyte-specific responses using standard
62 molecular and biochemical assays on bulk tissue. As a result, the underlying acid-base
63 and physiological causes of OA-induced otolith overgrowth remain unknown.

64 The chemistry of the endolymph is actively controlled by the inner ear epithelium
65 to maintain acid-base conditions that promote biomineralization, namely, higher pH,
66 $[HCO_3^-]$, $[CO_3^{2-}]$, and total CO_2 than the blood (Payan et al., 1999, 1997; Takagi, 2002;
67 Takagi et al., 2005). This gradient is actively maintained by two types of ion-transporting
68 cells (“ionocytes”): the Type-I ionocyte, which transports K^+ and Cl^- into the endolymph
69 and removes H^+ powered by Na^+/K^+ -ATPase (NKA) (Kwan et al., 2020; Mayer-Gostan

70 et al., 1997; Payan et al., 1997; Takagi, 1997) and the Type-II ionocyte, which secretes
71 HCO_3^- into the endolymph driven by V-type H^+ -ATPase (VHA) (Kwan et al., 2020;
72 Mayer-Gostan et al., 1997; Payan et al., 1997; Takagi, 1997; Tohse et al., 2006, 2004).
73 However numerous other cells within the inner ear organ also express NKA and VHA,
74 including the sensory hair cells and the endothelial cells that make up the blood vessels
75 (Kwan et al., 2020; Mayer-Gostan et al., 1997; Shiao et al., 2005).

76 In the current study, splitnose rockfish (*Sebastes diploproa*) were exposed to
77 $\sim 1,600 \mu\text{atm CO}_2$ (pH ~ 7.5), a condition readily experienced in their natural habitat
78 (Culberson and Pytkowicz, 1970; Love et al., 2002) and predicted for the surface ocean
79 by the year 2300 (Goodwin et al., 2018). The OA exposure spanned three days, a
80 duration previously documented to result in otolith overgrowth in fish larvae (Faria et al.,
81 2017). Blood acid-base chemistry was measured after taken samples using a
82 benzocaine-based anesthetic protocol that yields measurements comparable to those
83 achieved using cannulation (Montgomery et al., 2019). Additionally, we took advantage
84 of the large rockfish inner ear organ to collect sufficient endolymph for acid-base
85 chemistry analysis, and inner ear tissue for quantification of NKA and VHA protein
86 abundances. Finally, we performed immunohistochemical analyses on six inner ear cell
87 types to explore potential cell-specific changes in protein expression patterns. This
88 multidimensional approach allowed us to explore the mechanistic acid-base causes that
89 underlie otolith overgrowth in fish exposed to OA.

90

91 **Methods**

92 *Specimens*

93 Juvenile splitnose rockfish (*S. diploproa*) were caught from drifting kelp paddies
94 off the shores of La Jolla and raised in the Hubbs Experimental Aquarium (La Jolla,
95 USA) in accordance to the permit (#SCP13227) issued by the California Department of
96 Fish and Wildlife. Rockfish were raised for >2 years in a flow-through system with
97 seawater continuously pumped from the Scripps Coastal Reserve, and were fed frozen
98 market squids and food pellets (EWOS, Cargill Incorporated, Minneapolis, MN, USA).
99 Average rockfish total length (12.33 ± 0.16 cm) and weight (49.11 ± 2.18 g) (N=9) were
100 not significantly different between treatments. All experiments were approved under the
101 Institutional Animal Care and Use Committee protocol (#S10320) by the Scripps
102 Institution of Oceanography, University of California San Diego animal care committee.
103

104 *Experimental Aquarium Setup*

105 Two header tanks were supplied with ambient seawater from the Scripps Coastal
106 Reserve, one was not manipulated and was considered as the control condition. The
107 other header tank was bubbled with CO₂ using a pH-stat system (IKS Aquastar,
108 Karlsbad, Germany) to maintain a seawater pH ~7.5 and generate the OA condition.
109 Temperature and pH were continuously monitored and recorded every 2 minutes using
110 the IKS Aquastar system (figure S1). Discrete seawater samples were collected from
111 header tanks at the beginning and end of each experiment, and analyzed for alkalinity
112 (via titration with LabView software Version 2.9j; National Instruments, Austin, Texas,
113 United States), pH (using the indicator dye purified m-cresol purple (Liu et al., 2011) in
114 an Agilent 8453 spectrophotometer (Agilent, Santa Clara, CA, USA)), and salinity (by
115 converting density measurements using Mettler Toledo DE-45 (Mettler-Toledo,

116 Columbus, Ohio, United States)) by the Dickson Lab (Scripps Institution of
117 Oceanography). The pH values from the discrete seawater samples were used to
118 validate and back-correct the IKS pH measurements. Subsequently, the pH, alkalinity,
119 and salinity values were used to calculate $p\text{CO}_2$ using CO2SYS (Lewis and Wallace,
120 1998). These analyses indicated control pH and $p\text{CO}_2$ levels of 7.89 ± 0.012 and 571.90
121 $\pm 4.88 \mu\text{atm}$, respectively, which are typical for La Jolla, USA (Frieder et al., 2012;
122 Hofmann et al., 2011; Takeshita et al., 2015). In contrast, pH and $p\text{CO}_2$ in the OA
123 treatment were 7.49 ± 0.01 and $1,591.56 \pm 18.58 \mu\text{atm}$, respectively (table S1).

124 Each header tank supplied water to three opaque 3-L experimental tanks at a
125 flow rate of 0.3-L min^{-1} . Individual rockfish were acclimated within an experimental tank
126 for 12 hours, followed by a 72-hour exposure to control or OA conditions. To ensure
127 similar metabolic state among individuals, rockfish were not fed during the 48 hours
128 prior to the acclimations or during the experiment. Three separate experiments were
129 conducted during March 2020, each time with three control and three OA-exposed fish.
130 No mortality was observed.

131

132 *Blood, endolymph, and inner ear sampling*

133 Sampling and acid-base determinations were performed in a temperature-
134 controlled room at 18°C (i.e. same as that of seawater). Fish were anesthetized by
135 stopping the seawater flow into the individual experimental tank and slowly adding
136 benzocaine through to achieve a final concentration of 0.15 g/L . After fish lost
137 equilibrium (~ 5 minutes), they were moved to a surgery table where the gills were
138 irrigated with aerated seawater from their respective treatment (control or OA)

139 containing benzocaine (0.05 g/L) using a pump (Harter et al., 2021; Montgomery et al.,
140 2019, 2022). Blood was drawn from the caudal vein using a heparinized syringe and pH
141 was immediately measured using a microelectrode (OrionTM PerpHecTTM RossTM,
142 ThermoFisher Scientific, Waltham, MA, USA). Next, blood was centrifuged for 1 minute
143 at 6,000xg using a microcentrifuge (VWR Kinetic Energy 26 Joules, Radnor, PA, USA),
144 and the resulting plasma was measured for total CO₂ (TCO₂) using a carbon dioxide
145 analyzer (Corning 965, Ciba Corning Diagnostic, Halstead, Essex, United Kingdom).
146 After blood sampling (N=8-9), the fish was euthanized by spinal pithing, and the gills
147 were quickly removed. Endolymph (N=7-8) was drawn using a heparinized syringe from
148 the ventral side of the skull, and pH and TCO₂ were measured as described above.
149 CO₂ loss was minimized by measuring endolymph within 3 minutes after spinal pithing.
150 Inner ear tissue was either flash frozen in liquid nitrogen and stored at -80°C, or fixed in
151 4% paraformaldehyde (8 hours at 4°C), incubated in 50% ethanol (8 hours at 4°C), then
152 stored in 70% ethanol until processing.

153

154 *HCO₃⁻, CO₃²⁻, and pCO₂ calculation*

155 Blood and endolymph pH and TCO₂ values were used to calculate [HCO₃⁻],
156 [CO₃²⁻], and pCO₂ using the Henderson-Hasselbalch equation. The solubility coefficient
157 of CO₂ (plasma: 0.0578 mmol L⁻¹ Torr⁻¹; endolymph: 0.0853 mmol L⁻¹ Torr⁻¹), ionic
158 strength (plasma: 0.15 mol L⁻¹, endolymph: 0.18 mol L⁻¹), pK₁' (plasma: ~6.20,
159 endolymph: ~6.16), and pK₂' (plasma: ~9.76, endolymph: ~9.71) were based upon
160 (Boutilier et al., 1984) and (Takagi, 2002) for blood and endolymph, respectively. The

161 [Na⁺] (plasma: 170 mmol L⁻¹, endolymph: 100 mmol L⁻¹) used for calculating pK_{1'} was
162 based upon (Payan et al., 1997).

163

164 *Antibodies*

165 NKA was immunodetected using a monoclonal α 5 mouse antibody raised against
166 the α -subunit of chicken NKA (a5, Developmental Studies Hybridoma Bank, Iowa City,
167 IA, USA; (Lebovitz et al., 1989)), whereas the β -subunit of VHA was immunodetected
168 using a custom-made polyclonal rabbit antibody (epitope: AREEVPGRRGFPYGC;
169 GenScript, Piscataway, USA). These antibodies have been previously used in the inner
170 ear of the Pacific chub mackerel (*Scomber japonicus*; (Kwan et al., 2020)), and were
171 validated here for splitnose rockfish (figure S2). Secondary antibodies goat anti-mouse
172 HRP-linked secondary antibodies (Bio-Rad, Hercules, CA, USA) and goat anti-rabbit
173 HRP-linked secondary antibodies (Bio-Rad) were used for immunoblotting.

174

175 *Western Blotting and Relative Protein Abundance Analysis*

176 Frozen inner ear samples were immersed in liquid nitrogen, pulverized using a
177 handheld motorized homogenizer (Kimble®/Kontes, Dusseldorf, Germany), and
178 suspended in ice-cold homogenization buffer containing protease inhibitors (250 mmol
179 L⁻¹ sucrose, 1 mmol L⁻¹ EDTA, 30 mmol L⁻¹ Tris, 10 mmol L⁻¹ benzamidine hydrochloride
180 hydrate, 1 mmol L⁻¹ phenylmethanesulfonyl fluoride, 1 mmol L⁻¹ dithiothreitol, pH 7.5).
181 Samples were centrifuged at low speed (3,000xg, 10 minutes, 4°C) to remove debris,
182 and the resulting supernatant was considered the crude homogenate. Total protein
183 concentration in all fractions was determined by the Bradford assay (Bradford, 1976).

184 Prior to SDS-electrophoresis, samples were mixed with an equal volume of 90% 2x
185 Laemmli buffer and 10% β -mercaptoethanol, and heated at 70°C for 5 minutes. Proteins
186 (crude homogenate: 10 μ g per lane; membrane-enriched fraction: 5 μ g per lane) were
187 loaded onto a 7.5% polyacrylamide mini gel (Bio-Rad, Hercules, CA, USA) – alternating
188 between control and high CO₂ treatments to avoid possible gel lane effects. The gel ran
189 at 200 volts for 40 minutes, and the separated proteins were then transferred to a
190 polyvinylidene difluoride (PVDF) membrane using a wet transfer cell (Bio-Rad) at 100
191 mAmps at 4°C overnight. PVDF membranes were incubated in tris-buffered saline with
192 1% tween (TBS-T) with milk powder (0.1 g/mL) at RT for 1 hour, then incubated with
193 primary antibody (NKA: 10.5 ng/ml; VHA: 3 μ g/ml) in blocking buffer at 4°C overnight.
194 On the following day, PVDF membranes were washed with TBS-T (three times; 10
195 minutes each), incubated in blocking buffer with their respective secondary antibodies
196 (1:10,000) at RT for 1 hour, and washed again with TBS-T (three times; 10 minutes
197 each). Bands were made visible through addition of ECL Prime Western Blotting
198 Detection Reagent (GE Healthcare, Waukesha, WI) and imaged and analyzed in a
199 BioRad Universal III Hood using Image Lab software (version 6.0.1; BioRad). Following
200 imaging, the PVDF membrane was incubated in Ponceau stain (10 minutes, room
201 temperature) to estimate protein loading. Relative protein abundance (N=6-8) were
202 quantified using the Image Lab software (version 6.0.1; BioRad) and normalized by the
203 protein content in each lane.

204

205 *Whole-mount immunohistochemistry and confocal microscopy*

206 Immunolabeling was performed based on the protocol described in Kwan *et al.*,
207 (2020) for tissue sections and optimized for whole tissues as follows. Fixed inner ear
208 tissue was rehydrated in phosphate buffer saline + 0.1% tween (PBS-T) for 10 min.
209 Autofluorescence was quenched by rinsing in ice-cold PBS-T with sodium borohydride
210 (1.5 mg/mL; six times; 10 minutes each), followed by incubation in blocking buffer (PBS-
211 T, 0.02% normal goat serum, 0.0002% keyhole limpet hemocyanin) at room
212 temperature for one hour. Samples were incubated with blocking buffer containing
213 primary antibodies (NKA: 40 ng/mL; VHA: 6 µg/mL) at 4°C overnight. On the following
214 day, samples were washed in PBS-T (three times at room temperature; 10 minutes
215 each), and incubated with the fluorescent secondary antibodies (1:500) counterstained
216 with DAPI (1 µg/mL) at room temperature for 1 hour. Samples were washed again in
217 PBS-T as before and stored at 4°C until imaging.

218 Immunostained inner ear samples were immersed in PBS-T, mounted onto a
219 depressed glass slide fitted with a glass cover slip (No. 1.5, 0.17 mm) and imaged using
220 a Zeiss LSM800 inverted confocal microscope equipped with a Zeiss LD LCI Plan-
221 Apochromat 40x/1.2 Imm Korr DIC M27 objective and Zeiss ZEN 2.6 blue edition
222 software (Cambridge, United Kingdom). The following channels were used for imaging:
223 VHA (excitation 493 nm with 1% laser power, emission 517 nm, detection 510–575
224 nm), NKA (excitation 577 nm at 1% laser power, emission 603 nm, detection 571–617
225 nm), and DAPI (excitation 353 nm at 0.7% laser power, emission 465 nm, detection
226 410–470 nm). Z-stacks (range: ~70–400 optical sections; thickness: ~0.27 µm per
227 section) of the various inner ear cell types were visualized as maximum intensity
228 projection, and through orthogonal cuts to capture fluorescent signal across the X-Z and

229 Y-Z planes. Inner ear organs from four control and four OA-exposed rockfish were
230 imaged.

231

232 *Statistical Analysis*

233 Normality was tested using the Shapiro-Wilk normality test, and homogeneity
234 was tested using the F-test. Datasets that failed to meet the assumptions of normality
235 were log- (i.e. $[CO_3^{2-}]$, pH) or inverse-transformed (i.e. $[H^+]$). Acid-base parameters were
236 analyzed using two-way analysis of variance (2-way ANOVA), with “CO₂ level” (control
237 or OA) and “internal fluid” (blood or endolymph) as factors. If significant interaction
238 effect was detected, subsequent Tukey honest significant difference (HSD) tests were
239 used. NKA and VHA protein abundances were analyzed using two-tailed Student’s t-
240 tests. Values are reported as mean \pm s.e.m., and an alpha of 0.05 was employed for all
241 analyses. Statistical tests were performed using Prism (version 7.0a) and R (version
242 4.0.3; R Development Core Team, 2013).

243

244 **Results and discussion**

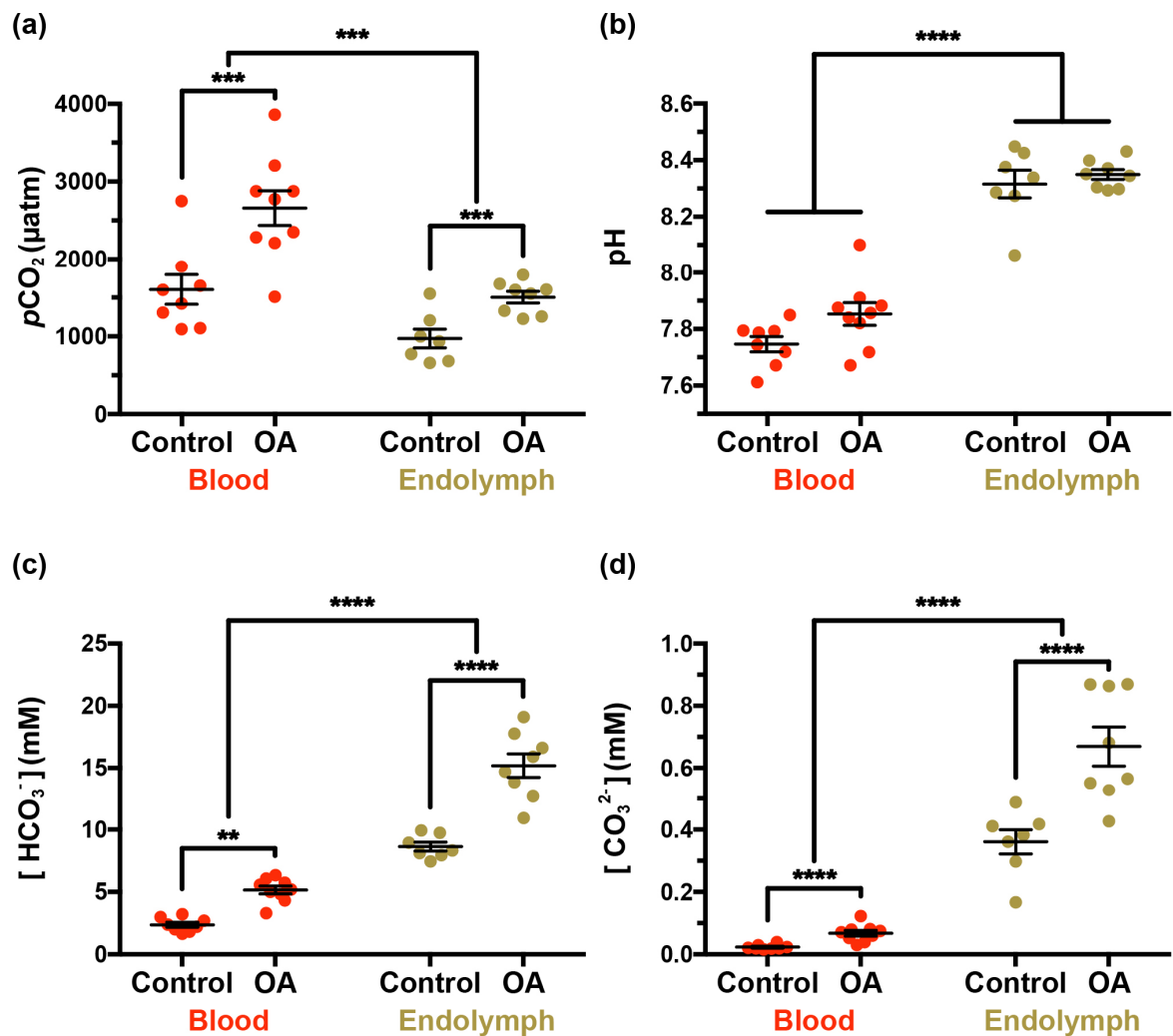
245 The difference in seawater pCO_2 between the control and OA-condition was
246 $\sim 1,000 \mu\text{atm}$, which induced an equivalent elevation in blood pCO_2 from $1,603.25 \pm$
247 $190.69 \mu\text{atm}$ in control fish to $2,659.20 \pm 223.87 \mu\text{atm}$ in OA-exposed fish (figure 1a).
248 However, blood pH was fully regulated (control: 7.75 ± 0.03 ; OA: 7.85 ± 0.04) (figure
249 1b). As is typical for regulation of blood acidosis (Tresguerres and Hamilton, 2017), OA-
250 exposed fish demonstrated a significant accumulation of HCO_3^- in blood plasma, from
251 $2.37 \pm 0.20 \text{ mM}$ in control fish up to $5.16 \pm 0.31 \text{ mM}$ in OA-exposed fish (figure 1c). This

252 response matches the magnitude of the hypercapnic stress according to classic
253 Davenport acid-base physiology, as well as the three previous studies on blood acid-
254 base chemistry in fish exposed to OA-relevant CO₂ levels (Esbaugh et al., 2016, 2012;
255 Montgomery et al., 2019). In addition, the increased plasma TCO₂ at unchanged pH led
256 to the tripling of plasma [CO₃²⁻] from ~0.02 to ~0.07 mM (figure 1d). These increases in
257 blood [HCO₃⁻] and [CO₃²⁻] may contribute to the skeletal hypercalcification (Di Santo,
258 2019) and deformities (Pimentel et al., 2014) reported in some OA-exposed fishes.

259 The endolymph of control rockfish had higher TCO₂ compared to the blood (9.06
260 \pm 0.38 vs 2.46 \pm 0.20 mM; figure S3) and also a higher pH (8.32 \pm 0.05 vs. 7.75 \pm 0.03),
261 resulting in lower *p*CO₂ (971.38 \pm 120.70 vs. 1,603.25 \pm 190.69 μ atm), higher [HCO₃⁻]
262 (8.63 \pm 0.35 vs. 2.37 \pm 0.20 mM), and much higher [CO₃²⁻] (0.36 \pm 0.04 vs 0.02 \pm 0.01
263 mM) (figure 1a-d). Importantly, these measurements revealed higher pH and lower
264 *p*CO₂, TCO₂, [HCO₃⁻] and [CO₃²⁻] compared to previous studies that collected
265 endolymph without previously anesthetizing the fish (Payan et al., 1999, 1997), and to
266 others that used 2-phenoxyethanol as anesthetic but did not irrigate the gills during
267 endolymph collection (Takagi, 2002; Takagi et al., 2005) (table S2). This finding
268 highlights the crucial importance of sampling procedures for accurate acid-base
269 measurements in fish physiological fluids. Indeed, fish struggling during handling and
270 hypoxia due to gill collapse during emersion are known to greatly affect blood acid-base
271 measurements, and our results indicate that these disturbances extend to the
272 endolymph.

273

274 In rockfish exposed to OA, endolymph $p\text{CO}_2$ increased from 971.38 ± 120.70 to
275 1503.21 ± 73.72 μatm (figure 1a). Crucially, this ~ 500 μatm increase was half of that
276 observed in the blood and therefore the $p\text{CO}_2$ difference between blood and endolymph
277 increased from ~ 600 to $\sim 1,100$ μatm , which is predicted to induce a proportional
278 increase in CO_2 flux into the endolymph following Fick's law of diffusion. Endolymph
279 TCO_2 in OA-exposed rockfish also nearly doubled (control: 9.06 ± 0.38 mM; OA: 15.96
280 ± 1.02 mM; figure S3) and, since pH remained unchanged at ~ 8.30 pH (figure 1b), it
281 was reflected as increased $[\text{HCO}_3^-]$ (control: 8.63 ± 0.35 mM, OA: 15.19 ± 0.95 mM vs)
282 (figure 1c) and $[\text{CO}_3^{2-}]$ (control: 0.36 ± 0.04 mM; OA 0.67 ± 0.06 mM) (figure 1d). Since
283 aragonite saturation state ($\Omega_{\text{aragonite}}$) is directly proportional to $[\text{CO}_3^{2-}]$, it implies that
284 biomineralization in the endolymph of OA-exposed fish is nearly twice more favorable
285 than in that of control fish. To our knowledge, this is the first direct evidence that the
286 acid-base chemistry in the endolymph of OA-exposed fish favors otolith overgrowth.
287



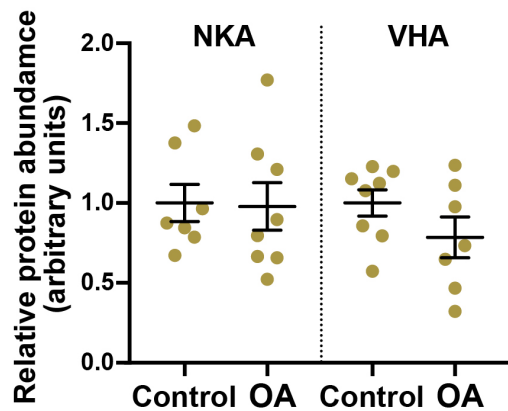
288

289 **Figure 1:** Blood and endolymph acid-base parameters in control and OA-exposed
290 rockfish. **A**) pCO_2 , **B**) pH, **C**) $[HCO_3^-]$, and **D**) $[CO_3^{2-}]$. Data is presented as mean and
291 s.e.m. for each group and the individual measurements are shown as red (blood) or
292 beige (endolymph) points (N= 7-9). Statistical significance between fluids, and between
293 treatments for a given fluid are indicated by the connecting lines and asterisks (2-way
294 ANOVA, *p<0.05, **p<0.005, ***p<0.001, ****p<0.0001). Statistical details are reported
295 in tables S3-S5, and TCO₂,[CO₂] and [H⁺] are shown in figure S3.

296

297 The increased $p\text{CO}_2$ diffusive rate into the endolymph and subsequent
298 generation of H^+ as a result of CO_2 hydration and CaCO_3 biomineralization would be
299 expected to induce a decrease in pH. Thus, the lack of change in endolymph pH in OA-
300 exposed rockfish indicates robust pH regulation. Hence, we hypothesized that OA-
301 exposed fish may have increased abundance of NKA and VHA, as these ATPases are
302 proposed to provide the driving force for transepithelial H^+ and HCO_3^- transport across
303 the inner ear epithelium (Kwan et al., 2020; Mayer-Gostan et al., 1997; Payan et al.,
304 1997; Shiao et al., 2005). However, Western blotting on bulk inner ear tissue revealed
305 no significant differences between control and OA-exposed fish (figure 2, table S6).

306



307
308 **Figure 2:** Na^+/K^+ -ATPase (NKA) and V-type H^+ -ATPase (VHA) protein abundance in
309 the inner ear organ of control and OA-exposed rockfish. Data is presented as mean and
310 s.e.m. and the individual measurements are shown as beige points ($N= 7-8$). Relative
311 protein abundance was calculated for each ATPase; NKA and VHA abundances are not
312 comparable to each other. There were no significant differences for NKA ($p=0.9104$) or
313 VHA ($p=0.1695$). Statistical details are reported in tables S6.

314

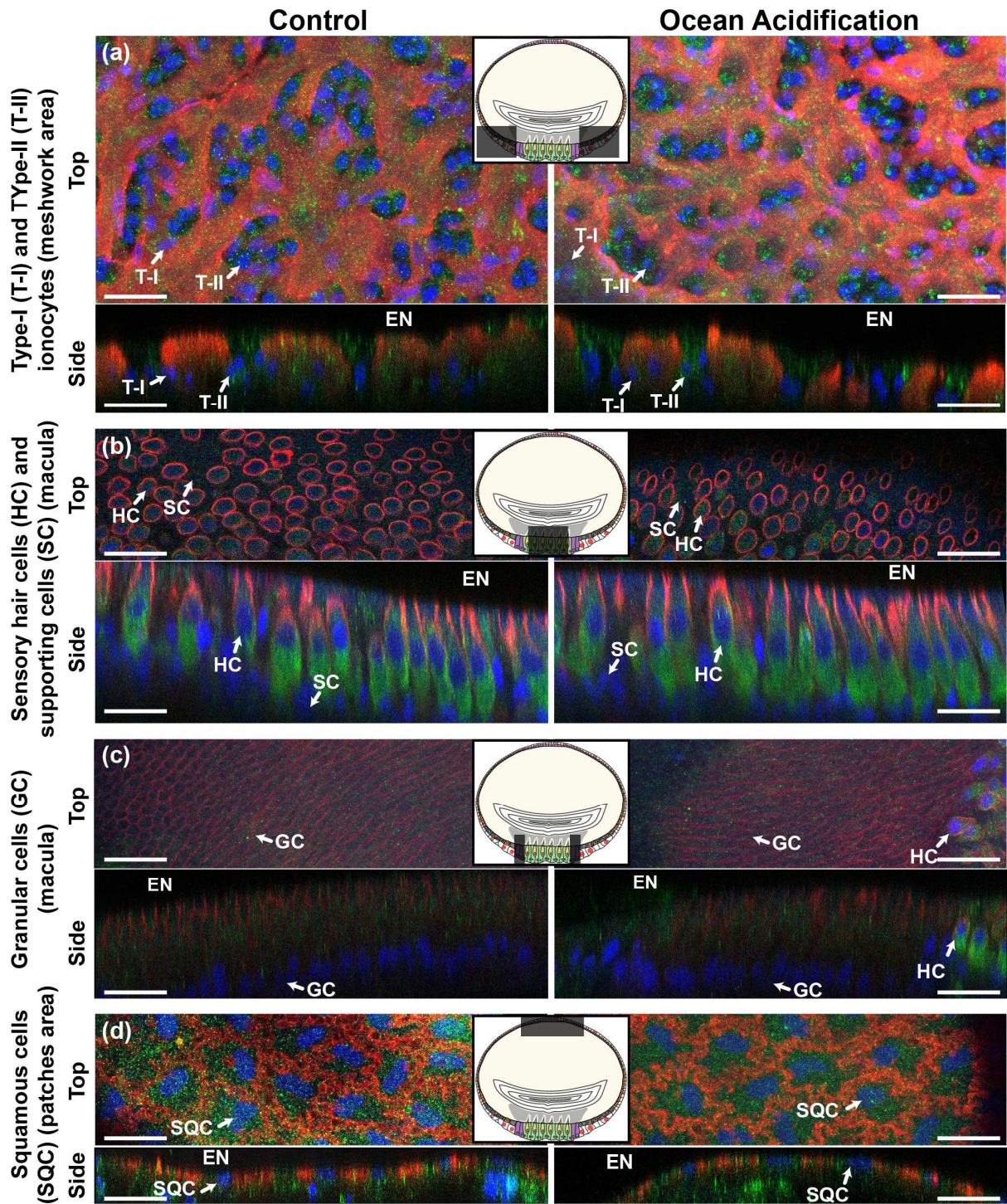
315 Next, we used immunocytochemistry and confocal microscopy to examine
316 potential changes in NKA and VHA abundance or sub-cellular localization in specific
317 inner ear epithelial cell types. The NKA and VHA immunostaining in rockfish inner ear
318 epithelial cells generally matched reports from other fish species (Kwan et al., 2020;
319 Pisam et al., 1998; Shiao et al., 2005; Takagi, 1997) (figure 3; figure S4), and there
320 were no apparent differences between control and OA-exposed fish in any cell type in
321 terms of signal intensity of subcellular localization. The Type-I ionocytes are
322 characterized by intense NKA signal in their highly infolded basolateral membrane and
323 by a much fainter cytoplasmic VHA signal (figure 3a). These ionocytes are most
324 abundant in the meshwork area, where they contact each other by their pseudopods
325 giving the appearance of an interconnected matrix. The Type-II ionocytes are
326 interspersed between the Type-I ionocytes in the meshwork area and have cytoplasmic
327 VHA signal of comparable intensity to that in the Type-I ionocytes; however, they lack
328 NKA signal (figure 3a). The sensory hair cells are in the macula; they express intense
329 NKA signal in their basolateral membrane and very intense cytoplasmic VHA signal,
330 which was especially concentrated towards their basal area consistent with synaptic
331 vesicles (figure 3b). The supporting cells surround each sensory hair cell; they display
332 faint cytoplasmic VHA signal and no detectable NKA signal (figure 3b). The granular
333 cells flank the macula and have a characteristic columnar shape. These cells have faint
334 NKA signal along their lateral plasma membrane and faint cytoplasmic VHA signal
335 (figure 3c). Finally, the squamous cells are found in the patches area in the distal side of
336 the epithelium; these cells are very thin and have NKA signal on their ribbon-like lateral

337 membrane as well as faint cytoplasmic VHA signal (figure 3d). A summary of the NKA
338 and VHA relative signal intensities in each cell type is reported in table S7.

339 The lack of apparent differences in NKA and VHA abundance and localization
340 cellular patterns between control and OA-exposed fish indicates that preexisting levels
341 of NKA and VHA were sufficient to mediate the endolymph pH regulation observed in
342 our study. Overall, these findings are consistent with models suggesting that H⁺
343 extrusion from the endolymph into the blood passively follows the transepithelial
344 potential that is established by active K⁺ excretion into the endolymph (Payan et al.,
345 2004). And since the function of the sensory hair cells requires a high [K⁺] in the
346 endolymph, modulation of inner ear transepithelial potential for the sole purpose of
347 decreasing H⁺ extrusion seems unlikely.

348 In our recent paper (Kwan et al., 2020), we proposed that HCO₃⁻ transport into
349 the endolymph and H⁺ removal could be upregulated by insertion of VHA into the
350 basolateral membrane of Type-II ionocytes; however, we found no evidence for such
351 mechanism in OA-exposed rockfish (figure 3a, *right panels*). Instead, upregulation of
352 ATPase activity could have occurred *via* other post-translational modifications or by
353 increased substrate availability (c.f. Kwan et al., 2021). The expression of carbonic
354 anhydrases, ion exchangers, and other acid-base relevant proteins must be examined
355 in future studies, ideally through an approach that includes cell-specific analyses. Lastly,
356 a contribution of non-bicarbonate buffering to endolymph pH regulation cannot be ruled
357 out; unfortunately, performing the required titrations are not trivial due to the small
358 volume of this fluid.

359



361 **Figure 3:** Immunocytochemistry of the inner ear epithelium of control and OA-exposed
362 rockfish. Na^+/K^+ -ATPase is in red, V-type H^+ -ATPase is in green, and nuclei are in blue.
363 There were no apparent differences in NKA or VHA signal intensities or localization

364 patterns between control and OA-exposed fish. **(a)** Type-I (T-I) and Type-II ionocytes
365 (T-II), **(b)** sensory hair cells (HC) and supporting cells (SC), **(c)** granular cells (GC), and
366 **(d)** squamous cells (SQC). The top view shows the X-Y plane in maximum projection,
367 whereas the side view shows the X-Z or Y-Z plane using orthogonal cuts. EN =
368 endolymph. Scale bar = 20 μ m. Images are representative of inner ear from four control
369 and four OA-exposed rockfish. The shaded boxes in the diagrams indicate the location
370 of each cell type within the otolith sac. A larger diagram showcasing the heterogeneous
371 cellular anatomy of the inner ear epithelium is provided in figure S4.

372

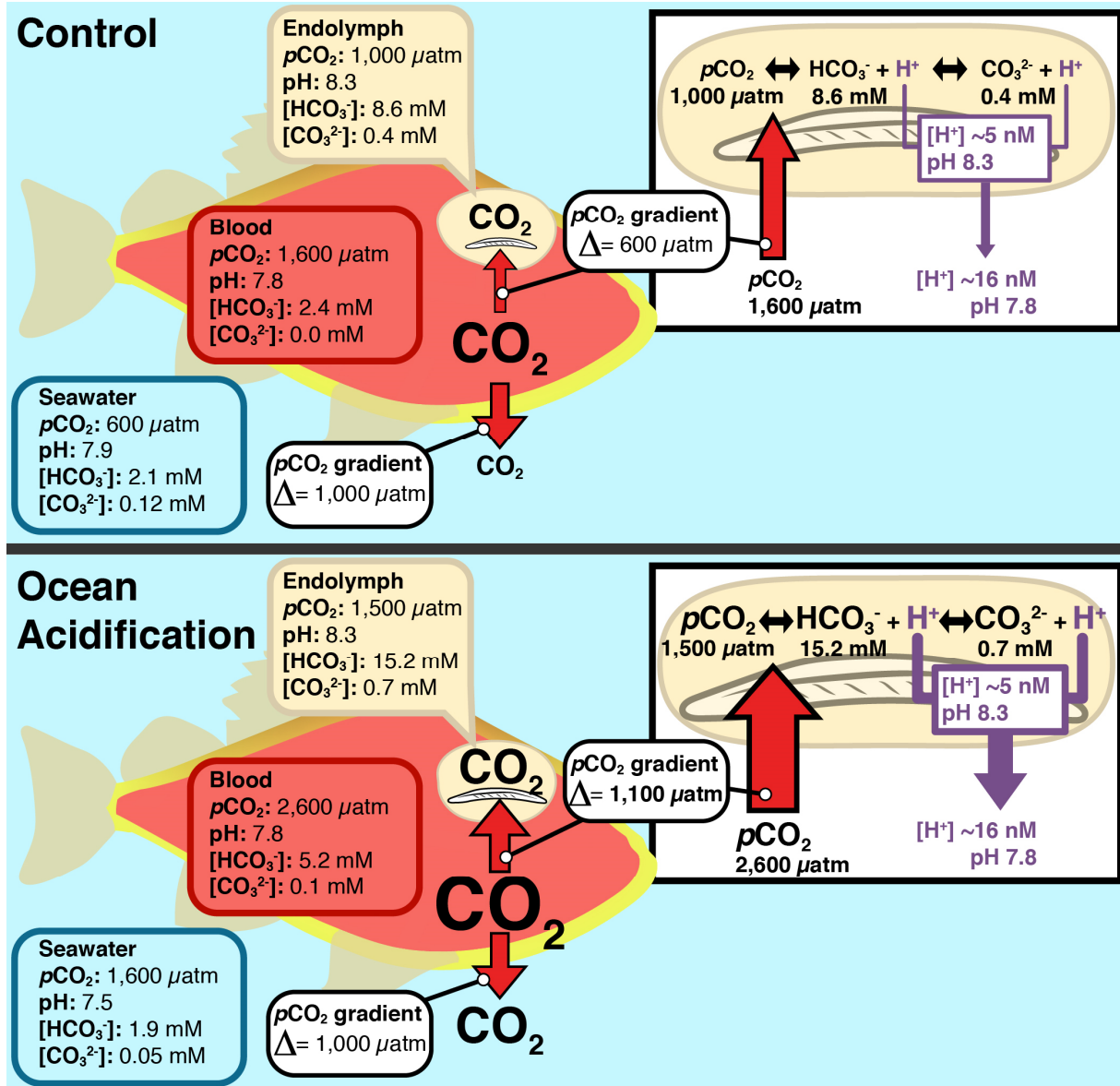
373 **Conclusions**

374 Increased endolymph $[HCO_3^-]$ and $[CO_3^{2-}]$ provides a mechanistic explanation for
375 otolith overgrowth in OA-exposed fish, a phenomenon that was first described over a
376 decade ago (Checkley et al., 2009). The ultimate cause is an interplay between blood
377 and endolymph acid-base regulation, which results in increased CO_2 flux into the
378 endolymph coupled with endolymph pH regulation. As a result, the carbonate equilibria
379 reactions shift to the right, promoting $[HCO_3^-]$ and $[CO_3^{2-}]$ accumulation bound to
380 increase $\Omega_{\text{aragonite}}$, and thus promote biomineralization (figure 4). This implies that otolith
381 overgrowth in response to OA will be more pronounced in fish species with more robust
382 acid-base regulatory mechanisms; however, this hypothesis must be experimentally
383 tested. Future studies should also investigate whether the fish inner ear epithelium can
384 curb otolith overgrowth during prolonged OA exposure, if the long-term response
385 requires changes in NKA and VHA protein abundance, and if species-specific
386 differences exist. Potential mechanisms include a change in the endolymph pH setpoint,

387 modulation of glycoprotein or Ca^{2+} secretion, and engagement of other compensatory
388 mechanisms. Coupled with functional studies (e.g. Radford et al., 2021; Shen et al.,
389 2016), this information will help predict whether the inner ear vestibular and auditory
390 sensory systems of fish will be affected by OA. Furthermore, understanding the
391 mechanisms responsible for otolith biomineralization and overgrowth during OA
392 exposure can help improve the accuracy of otolith-reliant aging techniques in the future
393 ocean.

394

395



396

397 **Figure 4:** Effect of blood and endolymph acid-base regulation on otolith overgrowth
398 during exposure to ocean acidification. Under control conditions, metabolically produced
399 CO₂ results in higher levels within the fish blood (~1,600 μatm) than those in seawater
400 (~600 μatm) and endolymph (~1,000 μatm). As a result, blood CO₂ diffuses into
401 seawater ($\Delta = \sim 1,000 \mu\text{atm}$) as it passes through the gills, and into the endolymph ($\Delta =$
402 $\sim 600 \mu\text{atm}$) as it passes through the inner ear. Under ocean acidification, the 1,000

403 μatm increase in seawater $p\text{CO}_2$ (to $\sim 1,600 \mu\text{atm}$) induces an equivalent increase in the
404 blood (to $\sim 2,600 \mu\text{atm}$), but a lesser increase in the endolymph (to $\sim 1,500 \mu\text{atm}$). Thus,
405 the $p\text{CO}_2$ diffusion gradient from the blood into seawater remain constant, but the $p\text{CO}_2$
406 diffusion gradient from the blood into the endolymph increases ($\Delta = \sim 1,100 \mu\text{atm}$). This
407 process is driven by pH regulation from the endolymph by the inner ear epithelium,
408 presumably by increased H^+ removal into the blood (although non-bicarbonate buffering
409 cannot be ruled out). The increased CO_2 diffusion rate into the endolymph coupled with
410 endolymph pH regulation results in the accumulation of $[\text{HCO}_3^-]$ and $[\text{CO}_3^{2-}]$, thereby
411 increasing $\Omega_{\text{aragonite}}$ and promoting otolith calcification. The size of the arrows is
412 proportional to the fluxes of CO_2 or H^+ .

413

414

415

416

417 **Acknowledgements**

418 This research was supported by National Science Foundation (NSF) grant IOS
419 #1754994 to M.T, and NSF Graduate Research Fellowship and NSF Postdoctoral
420 Research Fellowship in Biology (award #1907334) to GTK. We thank Phil Zerofski (SIO)
421 for collecting the fish and helping with aquarium matters. We are grateful to Taylor
422 Smith, Shane Finnerty, Gabriel Lopez, Kaelan Prime, and Dr. Till Harter for their help
423 with fish care. We also thank Kaelan Prime and Dr. Till Harter for their assistance with
424 experimental maintenance and sampling.

425

426

427

428 **Bibliography**

429

430 Bignami, S., Enochs, I.C., Manzello, D.P., Sponaugle, S., Cowen, R.K., 2013. Ocean
431 acidification alters the otoliths of a pantropical fish species with implications for
432 sensory function. *Proc. Natl. Acad. Sci.* 110, 7366–7370.
433 <https://doi.org/10.1073/pnas.1301365110>

434 Bignami, Sean, Sponaugle, S., Cowen, R.K., 2013. Response to ocean acidification in
435 larvae of a large tropical marine fish, *Rachycentron canadum*. *Glob. Chang. Biol.*
436 19, 996–1006. <https://doi.org/10.1111/gcb.12133>

437 Boutilier, R.G., Heming, T.A., Iwama, G.K., 1984. Appendix: Physicochemical
438 Parameters for use in Fish Respiratory Physiology**The authors were supported by
439 N.S.E.R.C. (Canada), in: Hoar, W.S., Randall, D.J. (Eds.), *Fish Physiology*.
440 Academic Press, pp. 403–430. [https://doi.org/https://doi.org/10.1016/S1546-5098\(08\)60323-4](https://doi.org/https://doi.org/10.1016/S1546-5098(08)60323-4)

442 Bradford, M.M., 1976. A rapid and sensitive method for the quantitation of microgram
443 quantities of protein utilizing the principle of protein-dye binding. *Anal. Biochem.* 72,
444 248–254. [https://doi.org/10.1016/0003-2697\(76\)90527-3](https://doi.org/10.1016/0003-2697(76)90527-3)

445 Campana, S.E., 2001. Accuracy, precision and quality control in age determination,
446 including a review of the use and abuse of age validation methods. *J. Fish Biol.* 59,
447 197–242. <https://doi.org/10.1006/jfbi.2001.1668>

448 Campana, S.E., Neilson, J.D., 1985. Microstructure of Fish Otoliths. *Can. J. Fish. Aquat.*
449 *Sci.* 42, 1014–1032.

450 Campana, S.E., Thorrold, S.R., 2001. Otoliths, increments, and elements: keys to a
451 comprehensive understanding of fish populations? *Can. J. Fish. Aquat. Sci.* 58, 30–
452 38. <https://doi.org/10.1139/cjfas-58-1-30>

453 Checkley, D.M., Dickson, A.G., Takahashi, M., Radich, J.A., Eisenkolb, N., Asch, R.,
454 2009. Elevated CO₂ enhances otolith growth in young fish. *Science* 324, 1683.
455 <https://doi.org/10.1126/science.1169806>

456 Culberson, C., Pytkowicz, R.M., 1970. Oxygen-total carbon dioxide correlation in the
457 Eastern Pacific Ocean. *J. Oceanogr. Soc. Japan* 26, 95–100.

458 <https://doi.org/10.1007/BF02753817>

459 Di Santo, V., 2019. Ocean acidification and warming affect skeletal mineralization in a
460 marine fish. *Proc. R. Soc. B Biol. Sci.* 286, 20182187.
461 <https://doi.org/10.1098/rspb.2018.2187>

462 Esbaugh, A.J., Ern, R., Nordi, W.M., Johnson, A.S., 2016. Respiratory plasticity is
463 insufficient to alleviate blood acid–base disturbances after acclimation to ocean
464 acidification in the estuarine red drum, *Sciaenops ocellatus*. *J. Comp. Physiol. B*
465 *Biochem. Syst. Environ. Physiol.* 186, 97–109. <https://doi.org/10.1007/s00360-015-0940-6>

466

467 Esbaugh, A.J., Heuer, R., Grosell, M., 2012. Impacts of ocean acidification on
468 respiratory gas exchange and acid-base balance in a marine teleost, *Opsanus*
469 *beta*. *J. Comp. Physiol. B* 182, 921–934. [https://doi.org/10.1016/0034-5687\(90\)90050-9](https://doi.org/10.1016/0034-5687(90)90050-9) <http://dx.doi.org/10.1007/s00360-012-0668-5>

470

471 Faria, A.M., Filipe, S., Lopes, A.F., Oliveira, A.P., Gonçalves, E.J., Ribeiro, L., 2017.
472 Effects of high pCO₂ on early life development of pelagic spawning marine fish.
473 *Mar. Freshw. Res.* 68, 2106. <https://doi.org/10.1071/MF16385>

474 Frieder, C.A., Nam, S.H., Martz, T.R., Levin, L.A., 2012. High temporal and spatial
475 variability of dissolved oxygen and pH in a nearshore California kelp forest.
476 *Biogeosciences* 9, 3917–3930. <https://doi.org/10.5194/bg-9-3917-2012>

477 Goodwin, P., Brown, S., Haigh, I.D., Nicholls, R.J., Matter, J.M., 2018. Adjusting
478 Mitigation Pathways to Stabilize Climate at 1.5°C and 2.0°C Rise in Global
479 Temperatures to Year 2300. *Earth's Futur.* 6, 601–615.
480 <https://doi.org/10.1002/2017EF000732>

481 Harter, T.S., Clifford, A.M., Tresguerres, M., 2021. Adrenergically induced translocation
482 of red blood cell β-adrenergic sodium-proton exchangers has ecological relevance
483 for hypoxic and hypercapnic white seabass. *Am. J. Physiol. Integr. Comp. Physiol.*
484 1–19. <https://doi.org/10.1152/ajpregu.00175.2021>

485 Heuer, R.M., Grosell, M., 2014. Physiological impacts of elevated carbon dioxide and
486 ocean acidification on fish. *AJP Regul. Integr. Comp. Physiol.* 307, R1061–R1084.
487 <https://doi.org/10.1152/ajpregu.00064.2014>

488 Hofmann, G.E., Smith, J.E., Johnson, K.S., Send, U., Levin, L.A., Micheli, F., Paytan,

489 A., Price, N.N., Peterson, B., Takeshita, Y., Matson, P.G., Crook, E.D., Kroeker,
490 K.J., Gambi, M.C., Rivest, E.B., Frieder, C. a., Yu, P.C., Martz, T.R., 2011. High-
491 frequency dynamics of ocean pH: a multi-ecosystem comparison. PLoS One 6,
492 e28983. <https://doi.org/10.1371/journal.pone.0028983>

493 Hurst, T.P., Fernandez, E.R., Mathis, J.T., Miller, J.A., Stinson, C.M., Ahgeak, E.F.,
494 2012. Resiliency of juvenile walleye pollock to projected levels of ocean
495 acidification. Aquat. Biol. 17, 247–259. <https://doi.org/10.3354/ab00483>

496 Ishimatsu, A., Hayashi, M., Kikkawa, T., 2008. Fishes in high-CO₂, acidified oceans.
497 Mar. Ecol. Prog. Ser. 373, 295–302. <https://doi.org/10.3354/meps07823>

498 Kalish, J.M., 1989. Otolith microchemistry: validation of the effects of physiology, age
499 and environment on otolith composition. J. Exp. Mar. Bio. Ecol. 132, 151–178.
500 [https://doi.org/10.1016/0022-0981\(89\)90126-3](https://doi.org/10.1016/0022-0981(89)90126-3)

501 Kwan, G.T., Shen, S.G., Drawbridge, M., Checkley, D.M., Tresguerres, M., 2021. Ion-
502 transporting capacity and aerobic respiration of larval white seabass (*Atractoscion*
503 *nobilis*) may be resilient to ocean acidification conditions. Sci. Total Environ. 791,
504 148285. <https://doi.org/10.1016/j.scitotenv.2021.148285>

505 Kwan, G.T., Smith, T.R., Tresguerres, M., 2020. Immunological characterization of two
506 types of ionocytes in the inner ear epithelium of Pacific Chub Mackerel (*Scomber*
507 *japonicus*). J. Comp. Physiol. B 190, 419–431. [01276-3](https://doi.org/10.1007/s00360-020-
508 01276-3)

509 Lebovitz, R.M., Takeyasu, K., Fambrough, D.M., 1989. Molecular characterization and
510 expression of the (Na⁺ + K⁺)-ATPase alpha-subunit in *Drosophila melanogaster*.
511 EMBO J. 8, 193–202.

512 Lewis, E., Wallace, D.W.R., 1998. CO2SYS dos program developed for CO₂ system
513 calculations.

514 Liu, X., Patsavas, M.C., Byrne, R.H., 2011. Purification and characterization of meta-
515 cresol purple for spectrophotometric seawater pH measurements. Environ. Sci.
516 Technol. 45, 4862–4868. <https://doi.org/10.1021/es200665d>

517 Love, M., Yaklovich, M., Thorsteinson, L., 2002. The Rockfishes of the Northeast
518 Pacific. UC Press, Berkeley.

519 Mayer-Gostan, N., Kossmann, H., Watrin, A., Payan, P., Boeuf, G., 1997. Distribution of

520 ionocytes in the saccular epithelium of the inner ear of two teleosts (*Oncorhynchus*
521 *mykiss* and *Scophthalmus maximus*). *Cell Tissue Res.* 289, 53–61.
522 <https://doi.org/10.1007/s004410050851>

523 Methot, R.D., 2015. Prioritizing Fish Stock Assessments. NOAA Tech. Memo. NMFS-
524 F/SPO- 152, 31 p.

525 Montgomery, D.W., Kwan, G.T., Davison, W.G., Finlay, J., Berry, A., Simpson, S.D.,
526 Engelhard, G.H., Birchenough, S.N.R., Tresguerres, M., Wilson, R.W., 2022. Rapid
527 blood acid-base regulation by European sea bass (*Dicentrarchus labrax*) in
528 response to sudden exposure to high environmental CO₂. *J. Exp. Biol.*
529 <https://doi.org/10.1242/jeb.242735>

530 Montgomery, D.W., Simpson, S.D., Engelhard, G.H., Birchenough, S.N.R., Wilson,
531 R.W., 2019. Rising CO₂ enhances hypoxia tolerance in a marine fish. *Sci. Rep.* 9,
532 1–10. <https://doi.org/10.1038/s41598-019-51572-4>

533 Pannella, G., 1971. Fish Otoliths : Daily Growth Layers and Periodical Patterns. *Science*
534 (80-). 173, 1124–1127.

535 Payan, P., De Pontual, H., Bœuf, G., Mayer-Gostan, N., 2004. Endolymph chemistry
536 and otolith growth in fish. *Comptes Rendus Palevol* 3, 535–547.
537 <https://doi.org/10.1016/j.crpv.2004.07.013>

538 Payan, P., Edeyer, A., de Pontual, H., Borelli, G., Boeuf, G., Mayer-Gostan, N., 1999.
539 Chemical composition of saccular endolymph and otolith in fish inner ear: lack of
540 spatial uniformity. *Am. J. Physiol.* 277, R123–R131.

541 Payan, P., Kossmann, H., Watrin, a, Mayer-Gostan, N., Boeuf, G., 1997. Ionic
542 composition of endolymph in teleosts: origin and importance of endolymph
543 alkalinity. *J. Exp. Biol.* 200, 1905–1912.

544 Pimentel, M.S., Faleiro, F., Dionisio, G., Repolho, T., Pousao-Ferreira, P., Machado, J.,
545 Rosa, R., 2014. Defective skeletogenesis and oversized otoliths in fish early stages
546 in a changing ocean. *J Exp Biol* 217, 2062–2070.
547 <https://doi.org/10.1242/jeb.092635>

548 Pisam, M., Payan, P., LeMoal, C., Edeyer, A., Boeuf, G., Mayer-Gostan, N., 1998.
549 Ultrastructural study of the saccular epithelium of the inner ear of two teleosts,
550 *Oncorhynchus mykiss* and *Psetta maxima*. *Cell Tissue Res.* 294, 261–270.

551 <https://doi.org/10.1007/s004410051176>

552 R Development Core Team, 2013. R: A language and environment for statistical
553 computing. R foundation for statistical computing.

554 Radford, C.A., Collins, S.P., Munday, P.L., Parsons, D., 2021. Ocean acidification
555 effects on fish hearing. *Proceedings. Biol. Sci.* 288, 20202754.
556 <https://doi.org/10.1098/rspb.2020.2754>

557 Réveillac, E., Lacoue-Labarthe, T., Oberhänsli, F., Teyssié, J.L., Jeffree, R., Gattuso,
558 J.P., Martin, S., 2015. Ocean acidification reshapes the otolith-body allometry of
559 growth in juvenile sea bream. *J. Exp. Mar. Bio. Ecol.* 463, 87–94.
560 <https://doi.org/10.1016/j.jembe.2014.11.007>

561 Shen, S.G., Chen, F., Schoppik, D.E., Checkley, D.M., 2016. Otolith size and the
562 vestibulo-ocular reflex of larvae of white seabass *Atractoscion nobilis* at high pCO₂.
563 *Mar. Ecol. Prog. Ser.* 553, 173–182. <https://doi.org/10.3354/meps11791>

564 Shiao, J.C., Lin, L.Y., Horng, J.L., Hwang, P.P., Kaneko, T., 2005. How can teleostean
565 inner ear hair cells maintain the proper association with the accreting otolith? *J.*
566 *Comp. Neurol.* 488, 331–341. <https://doi.org/10.1002/cne.20578>

567 Takagi, Y., 2002. Otolith formation and endolymph chemistry: A strong correlation
568 between the aragonite saturation state and pH in the endolymph of the trout otolith
569 organ. *Mar. Ecol. Prog. Ser.* 231, 237–245. <https://doi.org/10.3354/meps231237>

570 Takagi, Y., 1997. Meshwork arrangement of mitochondria-rich, Na⁺,K⁺-ATPase-rich
571 cells in the saccular epithelium of rainbow trout (*Oncorhynchus mykiss*) inner ear.
572 *Anat. Rec.* 248, 483–489. [https://doi.org/10.1002/\(SICI\)1097-0185\(199708\)248:4<483::AID-AR1>3.0.CO;2-N](https://doi.org/10.1002/(SICI)1097-0185(199708)248:4<483::AID-AR1>3.0.CO;2-N)

574 Takagi, Y., Tohse, H., Murayama, E., Ohira, T., Nagasawa, H., 2005. Diel changes in
575 endolymph aragonite saturation rate and mRNA expression of otolith matrix
576 proteins in the trout otolith organ. *Mar. Ecol. Prog. Ser.* 294, 249–256.
577 <https://doi.org/10.3354/meps294249>

578 Takeshita, Y., Frieder, C.A., Martz, T.R., Ballard, J.R., Feely, R.A., Kram, S., Nam, S.,
579 Navarro, M.O., Price, N.N., Smith, J.E., 2015. Including high-frequency variability in
580 coastal ocean acidification projections. *Biogeosciences* 12, 5853–5870.
581 <https://doi.org/10.5194/bg-12-5853-2015>

582 Tohse, H., Ando, H., Mugiya, Y., 2004. Biochemical properties and
583 immunohistochemical localization of carbonic anhydrase in the sacculus of the
584 inner ear in the salmon *Oncorhynchus masou*. Comp. Biochem. Physiol. - A Mol.
585 Integr. Physiol. 137, 87–94. [https://doi.org/10.1016/S1095-6433\(03\)00272-1](https://doi.org/10.1016/S1095-6433(03)00272-1)

586 Tohse, H., Murayama, E., Ohira, T., Takagi, Y., Nagasawa, H., 2006. Localization and
587 diurnal variations of carbonic anhydrase mRNA expression in the inner ear of the
588 rainbow trout *Oncorhynchus mykiss*. Comp. Biochem. Physiol. B. Biochem. Mol.
589 Biol. 145, 257–64. <https://doi.org/10.1016/j.cbpb.2006.06.011>

590 Tresguerres, M., Hamilton, T.J., 2017. Acid-base physiology, neurobiology and
591 behaviour in relation to CO₂ -induced ocean acidification. J. Exp. Biol. 220, 2136–
592 2148. <https://doi.org/10.1242/jeb.144113>

593 Vitale, F., Clausen, L.W., Chonchuir, G.N., 2019. Handbook of fish age estimation
594 protocols and validation methods. ICES Cooperative Research Report No. 346.
595 <https://doi.org/10.17895/ices.pub.5221>

596

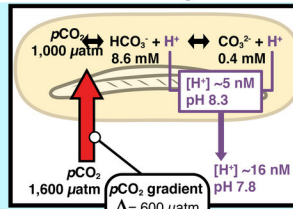
Rockfish exposed to ocean acidification (OA) regulated their blood and endolymph pH, which resulted in increased CO_2 diffusion into the endolymph and accumulation of bicarbonate and carbonate. This mechanism explains otolith overgrowth in fish exposed to OA, a phenomenon that was first reported in 2009. The links between blood and endolymph acid/base regulation in changing environments and otolith growth are also relevant for otolith-reliant fisheries techniques.

Control

Seawater
 $p\text{CO}_2$: 600 μatm
 pH: 7.9
 $[\text{HCO}_3^-]$: 2.1 mM
 $[\text{CO}_3^{2-}]$: 0.12 mM

Endolymph
 $p\text{CO}_2$: 1,000 μatm
 pH: 8.3
 $[\text{HCO}_3^-]$: 8.6 mM
 $[\text{CO}_3^{2-}]$: 0.4 mM

Blood
 $p\text{CO}_2$: 1,600 μatm
 pH: 7.8
 $[\text{HCO}_3^-]$: 2.4 mM
 $[\text{CO}_3^{2-}]$: 0.0 mM

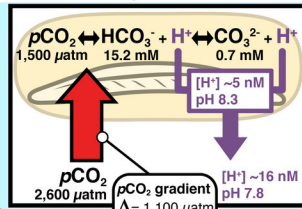


OA

Seawater
 $p\text{CO}_2$: 1,600 μatm
 pH: 7.5
 $[\text{HCO}_3^-]$: 1.9 mM
 $[\text{CO}_3^{2-}]$: 0.05 mM

Endolymph
 $p\text{CO}_2$: 1,500 μatm
 pH: 8.3
 $[\text{HCO}_3^-]$: 15.2 mM
 $[\text{CO}_3^{2-}]$: 0.7 mM

Blood
 $p\text{CO}_2$: 2,600 μatm
 pH: 7.8
 $[\text{HCO}_3^-]$: 5.2 mM
 $[\text{CO}_3^{2-}]$: 0.1 mM



The size of the arrows is proportional to the fluxes of CO_2 or H^+ .